Changes in the microstructure of wood smokes in a small aerosol chamber due to different factors

R.F. Rakhimov, E.V. Makienko, M.V. Panchenko, V.S. Kozlov, and V.P. Shmargunov

Institute of Atmospheric Optics, Siberian Branch of the Russian Academy of Sciences, Tomsk

Received December 29, 2002

We analyze the variations of optical and microphysical properties of aerosol formed due to thermal effect on the wood materials in closed volumes. Experiments show that, if an air mixture (with high concentration of aerosol particles and vapor of aerosol-bearing species) crosses temperature inhomogeneities many times, then two liquid droplet fractions form in the disperse composition of pyrolysis smokes with characteristic sizes $r \sim 0.55$ and 0.9 μm in the size interval of medium dispersed fraction (0.4–1.5 μm). The experiments revealed that, even in the case of a weak (~ 55°C) heating of surface of a coniferous tree wood, the achieved emission, with high concentration of aerosol particles and vapor of aerosol-bearing species (in closed volumes), has a rate quite sufficient for formation of finely dispersed fraction (0.05–0.2 μm) with optically measurable concentrations.

Introduction

The forest fires, aside from producing much heat over vast forested territories, also lead to activation of processes of thermal sublimation of volatile compounds and to stronger emission of aerosol-bearing gases (ABGs) from wood. The powerful heat sources result in more aerosols and ABGs uplifted from near-ground layer to the free atmosphere. Lifting and reaching regions with high temperature contrast, the ABGs, as part of air mixture, undergo complex phase transitions giving rise to high-concentration aerosol anomalies. Information on microstructure variations of disperse mixture is important for better understanding of the mechanism by which the smoke aerosol influences the optical and microphysical properties of tropospheric haze.

The paper analyzes the results of laboratory experiments aimed at studying the microstructure variations of dispersed mixture of particles, formed at the increase of concentration of vapor of aerosol-bearing species (VABSs), emitted by wood materials due to thermal heating.

1. Measurement and data processing technique

As in our previous study,[1] here the microstructure variations of smoke aerosol were analyzed through inversion of data of spectral measurements of scattering phase function (directional scattering coefficients (DSCs)) using a spectronephelometer. The DSC values were successively recorded at five fixed angles $\theta_i = 15$, 45, 110, 135, 165° and nine wavelengths in the spectral interval $\lambda_j = 0.44$–0.69 μm ($j = 1, \ldots, 9$). Rakhimov et al.[1] estimated the microstructure variations of smokes through solution of inverse problem using spectral values of the measured scattering phase function $\mu(\theta_i, \lambda_j)$ representing a sum of polarization components.

We took into account specific features of spectral variations of polarization DSC components, using 10 spectral dependences for $\mu_\perp(\theta_i, \lambda_j)$ and 10 for $\mu_{||}(\theta_i, \lambda_j)$ (two dependences for each angle).

The main instrumental features of the experiment have been discussed in detail in Refs. 1 and 2, which also discuss the method of preprocessing the measurement data. In the experiments addressed here the pyrolysis smokes were formed due to thermal decomposition of wood mass (less than 1 g) on heating element installed in small-size aerosol chamber of 0.1 m^3 volume. The temperature of air mixture in the chamber was controlled using two sensors. The heating level of sample in electric heating element was regulated by voltage supply U. The starting time of the experiments was synchronized at the moment of switching on of the heating element. The pyrolysis of all samples took 500 s. After smoke particle concentrations in the chamber were equalized, the smokes entered the spectronephelometer cell starting from 600 s. Upon reaching signal maximum (usually by 720–800 s), a program was initiated for automatic recording and storing of optical signals in computer memory. The wetting of disperse mixture in spectronephelometer cell was controlled with temperature and relative humidity sensors.

To determine the function $s(r) = \pi r^2 n(r)$ (in $\mu m/cm^3$), where $n(r) = dN/dr$ is the size distribution density of particle number concentration (in $\mu m^{-1}/cm^3$), we used a regularization algorithm based on approximation of the sought function by some step histogram $s^*(r)$ (Ref. 3). The function $s^*(r)$ is determined based on minimization of smoothing functional:

0235-6880/03/04 308-10 $02.00

$$F_\alpha = \sum_i^5 \eta_i \sum_j^9 \left(\sum_l^k q_{j,l} S_l - q_j \right)^2 +$$

$$+ \alpha \left[p_0 \sum_l^k S_l^2 + p_1 \sum_l^{k-1} (\Delta S_{l+1,\,l})^2 \right],$$

where p_0 and p_1 are scaling factors; α is regularization parameter; $\{q_{j,l}\}$ are elements of the matrix calculated from scattering efficiency factor $K(r, \lambda)$ for a given particle size and a corresponding scattering angle θ_k; η_i are weighting factors used to tune the relative significance of used spectral dependences for different scattering angles. The components of the vector of solution S_l represent total geometric particle cross section on intervals Δl with boundaries r'_l and r''_{l+1}. The mean value of step function $s^*(r)$ on this interval is given by S_l/Δ_l.

Figure 1 presents calculated scattering cross sections for different angles as functions of diffraction parameter $\rho = 2\pi r/\lambda$, where r is the particle radius in μm. These functional dependences are kernels of integral equation used in solution of the inverse problem to estimate the aerosol size spectrum. From the calculations presented in Fig. 2 we see that the shape of presented dependences changes significantly for the diffraction parameter n varying between 1.33 and 1.59. Thus, when this optical dataset is used as the initial information, the accuracy of estimates of smoke aerosol size spectrum depends substantially on the refractive index used. Special attention in the paper is given to justification of variability range of the refractive index, admissible in the experiments carried out.

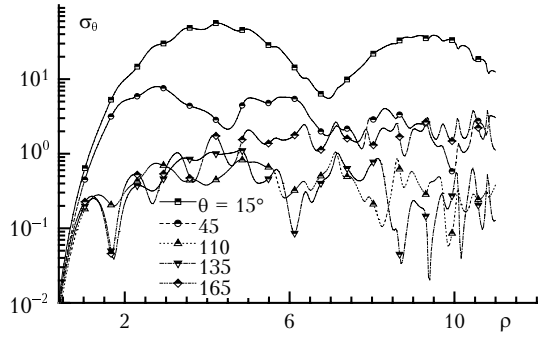

Fig. 1. Dependence of scattering efficiency factors $\sigma_\theta(\rho)$ on the diffraction parameter $\rho = 2\pi r/\lambda$ for different scattering angles θ.

Mean effective refractive index (average for analyzed size range of polydisperse ensemble of particles) was estimated for each realization of laboratory experiment, based on preliminary solution of inverse problem. First, we justified the boundaries of the interval for size spectrum $s(r)$, where it is positive definite. Then, using all measured spectral dependences, we determined the minimum of the functional $F_\alpha[s(r), m]$ on rectangular grid of values of real and imaginary parts of the refractive index (Fig. 3). Finally, the obtained estimates of the complex refractive index were used to ascertain the sought volume size distribution of smoke particles $v(r) = 4\pi r^3 n(r)/3 = dV/dr$ (in $\mu m^2/cm^3$).

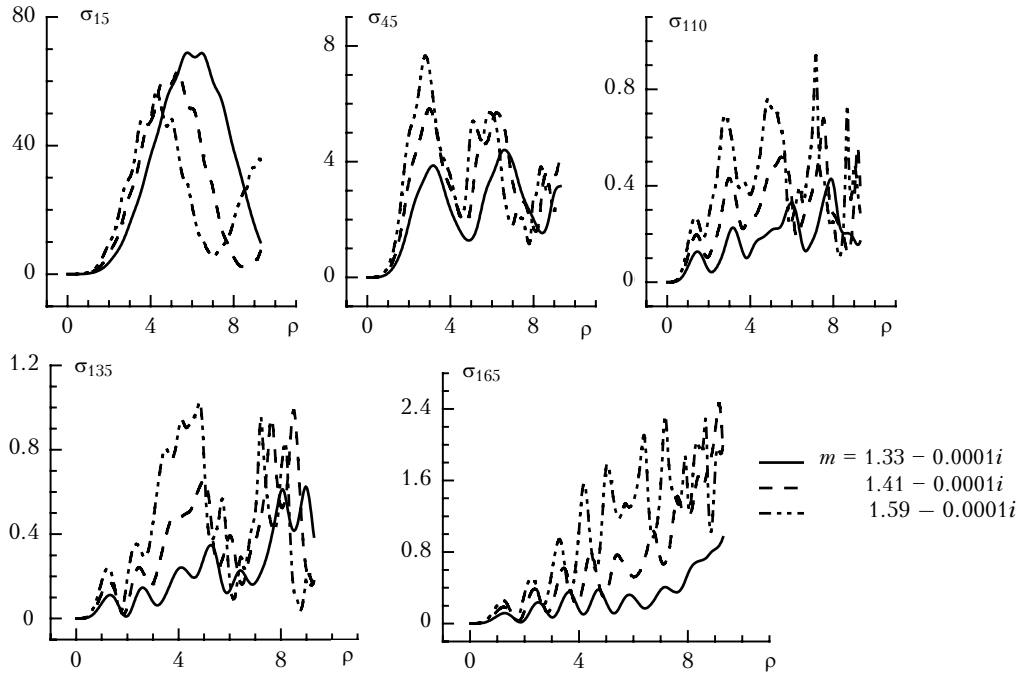

Fig. 2. Dependences of scattering efficiency factor $\sigma_\theta(\rho)$ for three values of the refractive index.

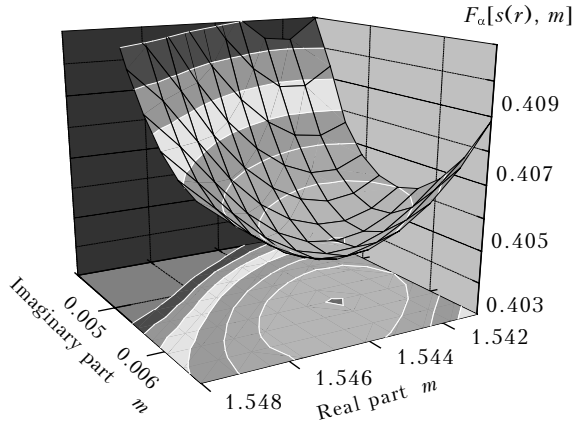

Fig. 3. Illustration of the algorithm of estimating the optimal value of the refractive index m of smoke particles through determination of the minimum of functional $F_\alpha[m, s(r)]$.

2. Results

Before studying the microstructure variations of smoke aerosols generated due to thermal effect on wood material, we analyzed extensively the variations of size spectrum and mean effective refractive index of aerosols formed due to heating of colophony (coniferous tar). This aerosol type was considered by many authors, and some microstructure features of these aerosols were reproduced many times.

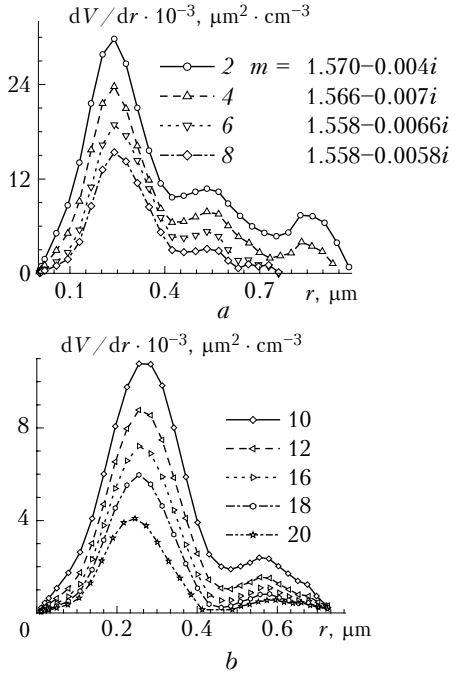

Fig. 4. Variations of volume particle size distribution for colophony smoke: (*a*) between second and eighth data points of optical signal recording (once ~ 7 min); and (*b*) between tenth and twentieth points.

The results of the study are presented in Fig. 4. First, the real part of refractive index estimated to be 1.58–1.55 satisfactorily agrees with data of other authors.[4,5] Secondly, the estimates revealed definite stable dynamics of variations of both parts of the refractive index. The obtained estimates give the value of single scattering albedo of ~ 0.90. The upper boundary of the size spectrum R_2 at the initial stage of process development reaches ~ 1.0 μm. Most of particles formed due to sublimation of coniferous tar in the chamber with air temperature T ~ 19–23°C and relative humidity RH ~ 35% have effective size ~ 0.16 μm.

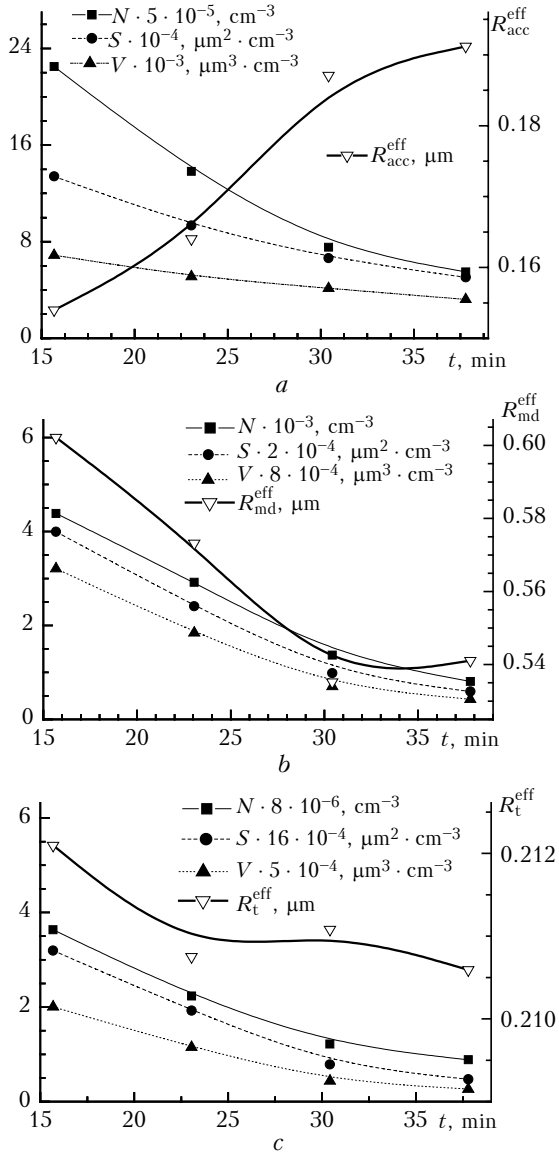

Fig. 5. Variations of integrated parameters of size spectrum, namely N_f, S_f, V_f, and effective size R_f^{eff} of smoke aerosols in different size ranges: (*a*) 0.05–0.39; (*b*) 0.4–1.0; and (*c*) 0.05–1.0 μm (subscripts of integrated characteristics "acc", "md", and "t" correspond to particle size ranges in order of increasing particle size).

In the course of measurements, the size spectrum of colophony smoke gradually looses the largest particle fraction, the size spectrum becomes narrower, and the upper boundary of the R_2 spectrum shifts toward ~ 0.6–0.7 μm. In the initial spectrum of volume

distribution, three maxima are consistently observed. The time behavior of the spectrum suggests that an effective particle sink to the chamber wall exists. The kinetic changes (coagulation growth) for the given level of particle concentration are insignificant against background of effective particle sink to the walls. Figure 5 presents variations of integrated characteristics of size spectrum, namely, number concentration N_f, total cross section S_f, and volume V_f, as well as effective particle size $R_{acc}^{eff} = 0.75V_f/S_f$ in the size range $r < 1.0$ μm. The values of characteristics are reduced to a common scale using corresponding factors indicated near each curve in Fig. 5.

Specific variations of N_f, S_f, and V_f characteristics in different size ranges reflect the tendencies of changes in the characteristic particle size. As seen from Fig. 5, with the increase of particle number concentration, the rate of increase of the effective size of tar particles R_{acc}^{eff} in size range discussed here gradually decelerates and finally becomes zero. Since then, the coagulation growth can no longer counterbalance the effective particle sink to the chamber walls and pipes delivering the disperse mixture to spectronephelometer cell.

The results of laboratory experiments have shown that the pyrolysis of wood materials (cedar, pine) leads to formation of smoke aerosols whose main microphysical parameters are similar to those from pyrolysis of colophony, but have more variable optical properties, especially at the initial stage. Figure 6 shows data sampled according to time variations of polarization degree for specific scattering angles in the experiments.

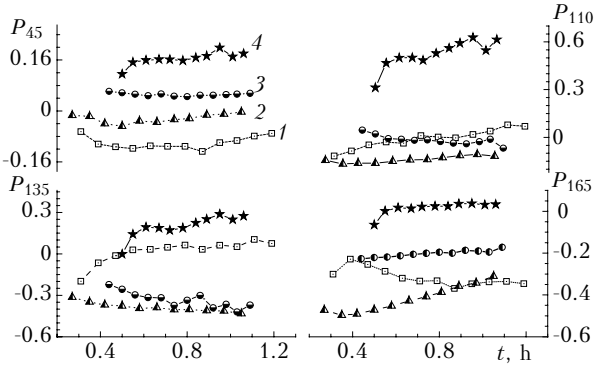

Fig. 6. Time variations of degree of polarization for specific scattering angles in the experiments: with wetted air mixture (curve *1*); with heating of chamber prior (curve *2*) and after pyrolysis of sample (curve *3*); emission of particles from chamber walls without pyrolysis of the sample (curve *4*).

For a preliminary cleaning of pyrolysis chamber, we used real atmospheric air mixture supplied through the window. To clean ambient air, we used aerosol filters of AFA type, which reduced significantly the content of particles with radii more than 0.1 μm. However, the temperature and relative humidity sensors, installed inside the measurement cell, indicated substantial variations of absolute humidity in air mixture used for cleaning, probably associated with specific synoptic and seasonal features during the experiments. This resulted in variability of obtained results. Figures 7*a* and *b* shows angular dependences of scattering phase function and degree of polarization for different wetting levels and air temperatures inside the measurement cell.

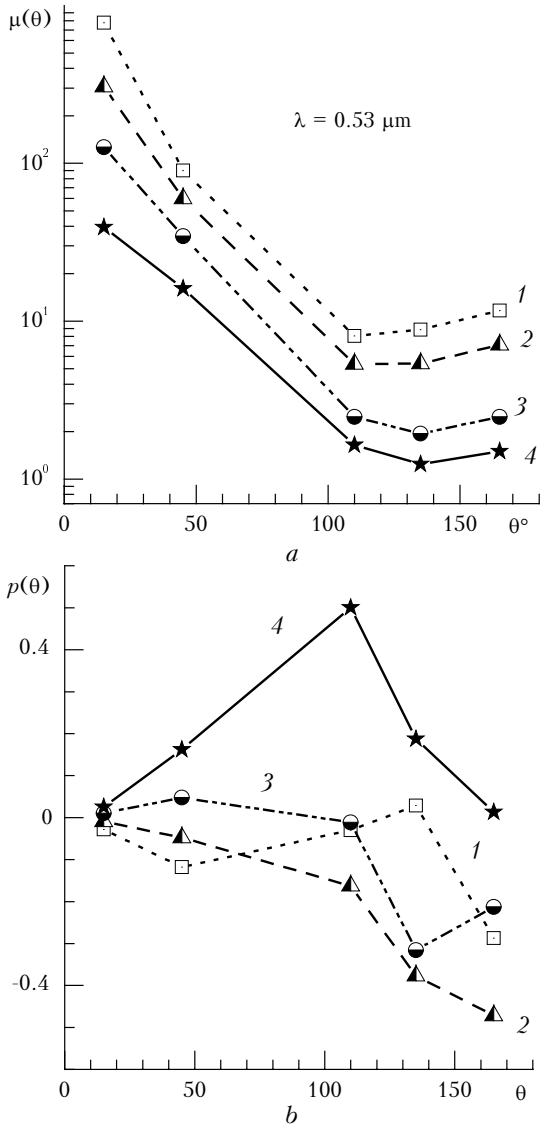

Fig. 7. Angular variations of directional scattering coefficients and degree of polarization (for λ = 0.53 μm) in different experiments. Symbols near curves correspond to those in Fig. 6.

Figure 8 shows microstructure data obtained during sublimation of cedar branches in the presence of needles (experiment 1). In this case, to produce a thermal effect on needles, the air temperature in small-size chamber was preliminarily raised from + 20 to + 50°C. The relative humidity inside the chamber was RH = 28% prior to heating and 43% after it. Then the chamber was filled with aerosol particles formed due to pyrolysis of cedar branches (without needles) inside the heating element at temperature ~ 470°C.

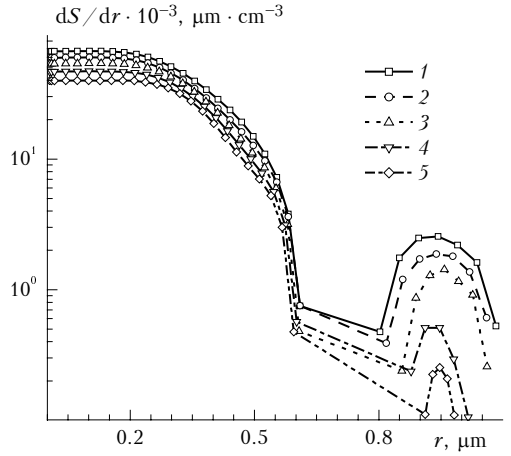

Fig. 8. Time variations of size distribution density of total cross section of smoke particles formed due to pyrolysis of cedar branches in chamber with heated needles. Curves *1–5* correspond to first five data points of optical signal recording with constant sampling rate between ~ 28 and 45 min of pyrolysis process.

The inversion results have shown that the best agreement with measurements is achieved using mean effective refractive index $m = 1.48–0.0003i$ for the principal mode of size spectrum and $m = 1.34–0.0001i$ for the second mode (with $r \sim 1$ μm). The former m value was obtained by determining the minimum of functional for the entire spectrum. The latter value of refractive index (for coarse particle fraction with fixed m for the main fraction, found at the first stage) was verified using analogous minimization algorithm on a variable grid of values of real and imaginary parts of the refractive index. The obtained estimates show that, whereas effective refractive index of principal mode is mostly determined by tar species, the composition of coarse fraction is dominated by water.

Figure 9 presents variations of integrated characteristics of size spectrum, namely N_f, S_f, V_f, as well as effective particle size R_f^{eff} in different size ranges. The obtained estimates suggest that the size spectrum of the principal mode (Fig. 9*a*), despite the marked decrease of the total aerosol content (see dynamics of variations of integrated characteristics of spectrum), shows small but stable increase of the mean particle size. The particles in medium dispersed size range (Fig. 9*b*) monotonically decrease in both content and size. Analogous data obtained for the whole spectrum are presented in Fig. 9*c*.

The conclusion that particles in one of the experiment are predominately water droplets follows not only from the fact that the refractive indices are close to those for water particles, but also from an additional experiment 2, designed to test this hypothesis.

Figure 10 presents the variations of volume particle size distribution reconstructed from results of dedicated experiment. In experiment 2, during pyrolysis generation of smokes from pine wood (450 mg in mass, heated to temperature 300°C) since 200 s, 40 water droplets (~ 2.2 g) were entered into

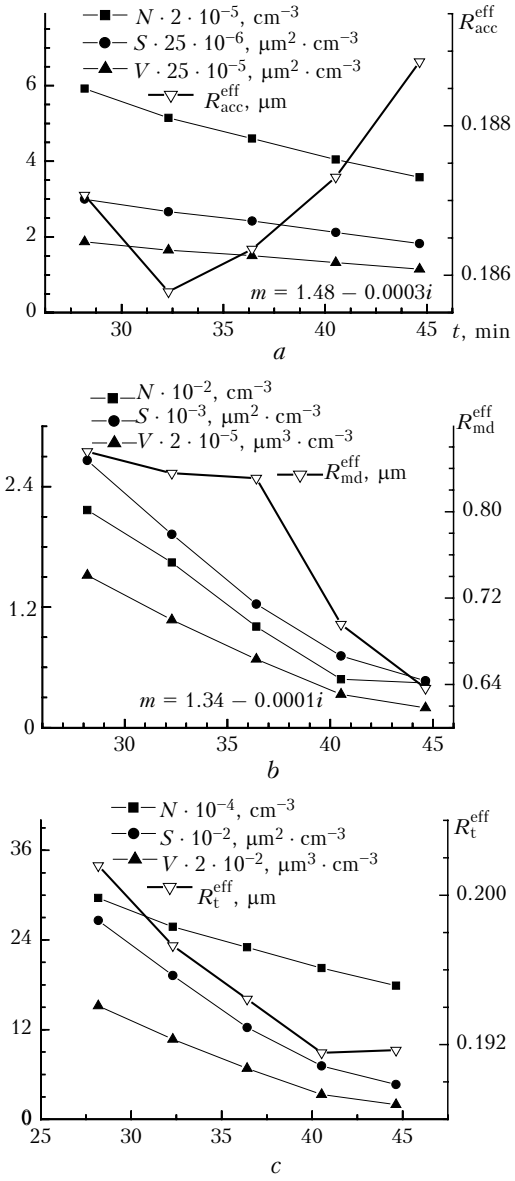

Fig. 9. Variations of integrated parameters of size spectrum, namely N_f, S_f, V_f, and effective size R_f^{eff} of aerosols formed due to pyrolysis of cedar branches in chamber with heated needles in size range (*a*) 0.05–0.61 μm; (*b*) 0.62–1.0 μm; and (*c*) 0.05–1.0 μm.

small-size chamber using dropper without preliminary heating of air mixture ($T_{\text{p.c}} = 29$°C); these droplets subsequently evaporated from preliminarily heated surface ($T_{\text{s}} \approx 60$°C). Considering that, in the beginning of the experiment, the absolute moisture content inside the chamber was 4.5 g · m^{-3}, the added water brought the air mixture to dew point inside the measurement cell, where air temperature dropped to + 19°C, i.e., relative humidity (inside the cell) reached ~ 100%. The gradual wetting of the chamber had an effect on variations of mean effective refractive index of main fraction of smoke particles, whose real part varied from 1.5 to 1.447. Simultaneously, consistent with the previous experiment, we again revealed the

water fraction of aerosol particles ~ 1.0 μm in size. In six cycles of signal recording, the total content of water particles gradually decreased and, by approximately seventh recorded data point, they were no longer recorded (against the background of experimental error). However, in the course of the same measurement cycle, the reconstructed spectra in size range 0.5–0.85 μm have gradually revealed a new aerosol fraction with the real part of the refractive index close to 1.33, characteristic of water particles.

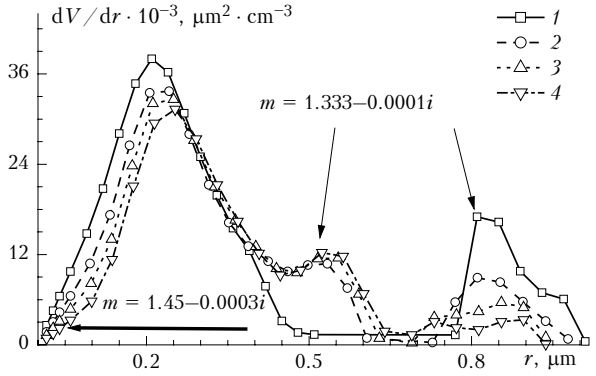

Fig. 10. Measurement of volume size distribution of particles formed in experiment with additional wetting of the chamber during pyrolysis of pine wood. Curves *1–4* correspond to first four data points of optical signal recording.

The performed experiments have such a scheme that, as smoke particles move from pyrolysis chamber to spectronephelometer cell and back, the aerosol-gaseous mixture crosses a few temperature inhomogeneities. As a result of thermal decomposition of wood sample in the crucible, the temperature inside small-size chamber increases by approximately 7–10°C, whereas in the cell of nephelometer the temperature remains close to room temperature. This was the case, for instance, in the experiments 1 and 2. The pyrolysis of wood material produced a concentrated aerosol-gaseous mixture which, via supply channels, was entered into the nephelometer cell, where, after rapid cooling, it experienced marked increase of relative humidity up to dew point, reflected in above-mentioned microstructure features of smoke in these experiments.

In experiments 3–9 the absolute moisture content inside small-size chamber was increased stepwise, so that the relative humidity *RH* of analyzed aerosol-gaseous mixture in the nephelometer cell was below dew point and varied from 40 to 95%. Bark-covered cuts from cedar branch were used as wood sample with mass 380 mg. The pyrolysis of samples was performed at one and the same voltage applied to the heating element.

It should be noted that, in implementation of measurement series discussed here, we revealed a number of factors affecting substantially the results, but not taken into account in preliminary development of the method of optical measurements. In particular, because of no control over specific content of wood tar in the sample, the initial indoor temperature, and temperature of air mixture inside the chamber, the temperature of pyrolysis markedly varied (±35°C relative to mean) in the range 390–460°C. The specific content of tar in the sample modulated production rate of both the aerosol particles and VABS. Changes of the initial indoor temperature produced marked variations of air temperature and relative air humidity inside the chamber and spectronephelometer cell. Generally, the mean initial temperature of air mixture inside the pyrolysis chamber was approximately (20 ± 3)°C. The temperature in chamber increased due to pyrolysis by 3–5°C, and due to wetting by another 4–7°C, averaging 28–31°C. Purposefully, the absolute moisture content inside the chamber was altered using a dropper. The vaporization of water was made through a weak heating of drop collector.

Table 1 presents variations of the integral characteristics of dispersed structure in different size ranges, describing measurements in experiments 3 and 8; these characteristics are obtained for extreme values of the relative humidity, found to be 45 and 91%, respectively.

From Table 1 we can easily see that, overall, the variations of integral characteristics, with minor excursions, follow the law of exponential decay:

$$V(t) = V_0 \exp(-a_V t).$$

At the same time, the rate of exponential decrease of smoke particle concentration, which is proportional to parameter a_V, markedly varies for different size ranges.

The results of performed series of measurements show that, in all experiments, the rate of variations of volume content of smoke particles in the size range 0.05–0.39 μm is generally lower than that of the total cross section of these particles. Therefore, even against background of effective aerosol sink to the chamber walls, the size spectrum of accumulation-mode fraction of smoke continues to shift toward larger sizes for some time, primarily due to coagulation particle growth.

A somewhat different variability pattern is characteristic of smoke particles in the size range 0.4–1.4 μm, where medium dispersed fraction forms. Earlier,[6,7] in interpretation of anomalous spectral dependence of atmospheric aerosol optical depth (AOD), we noted that particles in this size range play an important role. Particles in this size subrange are found in many atmospheric situations and have distinct diurnal variations of disperse composition.[8]

Analysis of time variations of integrated parameters of medium dispersed fraction indicates that the rate of decrease of the particle volume markedly exceeds that of decrease of the total cross section of these particles. In other words, independent of the state of relative humidity of air mixture, the effective particle size in a given size range usually steadily decreases (except in experiment 8).

Table 2 presents in columns 2–5 the values of coefficient a (in min^{-1}) obtained for $V(t)$ and $S(t)$ of accumulation and medium dispersed fractions. Columns 6 and 7 of this table present the differences $\Delta a = a_V - a_S$ corresponding to aerosol fractions discussed here; while columns 8–10 show the experimentally achieved maxima of relative and absolute humidity of air mixture inside the optical cell, as well as the temperature.

Table 1

	Accumulation-mode fraction $0.05 < r < 0.39$ μm				Medium dispersed fraction $0.4 < r < 1.4$ μm				Whole size spectrum $0.05 < r < 1.4$ μm				Temperature and relative humidity			
													Nephelometer cell		Pyrolysis chamber	
t, min	N_{acc}, cm^{-3}	S_{acc}, $\mu m^2 \cdot cm^{-3}$	V_{acc}, $\mu m^3 \cdot cm^{-3}$	R^{eff}_{acc}, μm	N_{md}, cm^{-3}	S_{md}, $\mu m^2 \cdot cm^{-3}$	V_{md}, $\mu m^3 \cdot cm^{-3}$	R^{eff}_{md}, μm	N_t, cm^{-3}	S_t, $\mu m^2 \cdot cm^{-3}$	V_t, $\mu m^3 \cdot cm^{-3}$	R^{eff}_t, μm	$T_{n.c}$, °C	$RH_{n.c}$, %	$T_{p.c}$, °C	$RH_{p.c}$, %
Experiment 3																
12	2.44E6*	3.32E5	1.15E4	0.104	1.23E4	7.12E4	1.61E4	0.680	2.45E6	4.03E5	2.76E4	0.206	18.3	46.0	33.6	19.5
15.7	1.55E6	2.57E5	9.85E3	0.115	9.82E3	5.06E4	1.08E4	0.640	1.56E6	3.08E5	2.06E4	0.201	18.4	50.0	33.2	21.8
19.4	1.12E6	2E5	7.85E3	0.118	7.66E3	3.4E4	6.73E3	0.594	1.13E6	2.34E5	1.46E4	0.187	18.5	49.3	32.8	22.1
23.1	8.61E5	1.6E5	6.46E3	0.121	5.32E3	2.2E4	4.21E3	0.574	8.67E5	1.82E5	1.07E4	0.176	18.5	48.5	32.3	22.4
26.7	6.01E5	1.27E5	5.5E3	0.130	2.95E3	1.13E4	2.07E3	0.551	6.04E5	1.38E5	7.57E3	0.164	18.6	47.8	31.9	22.6
30.4	4.28E5	9.58E4	4.26E3	0.133	2.6E3	8.05E3	1.33E3	0.496	4.31E5	1.04E5	5.59E3	0.162	18.7	47.0	31.5	22.9
34.1	3.06E5	7.29E4	3.34E3	0.138	1.98E3	5.22E3	797	0.458	3.08E5	7.81E4	4.14E3	0.159	18.8	46.3	31.1	23.2
Experiment 8																
12	1.11E6	4.52E5	2.72E4	0.180	3.18E3	3.34E4	1.02E4	0.915	1.11E6	4.86E5	3.74E4	0.231	18.4	56.0	33.9	23.5
15.7	8.89E5	3.64E5	2.19E4	0.180	1.51E3	1.84E4	6.05E3	0.984	8.9E5	3.82E5	2.79E4	0.219	18.5	85.0	33.0	37.8
19.4	6.38E5	2.67E5	1.62E4	0.182	700	8.79E3	2.93E3	0.999	6.39E5	2.76E5	1.92E4	0.208	18.6	88.0	32.0	41.5
23.1	4.89E5	2.24E5	1.43E4	0.191	343	4.3E3	1.43E3	0.998	4.89E5	2.29E5	1.57E4	0.206	18.8	91.0	31.2	45.3
26.7	3.48E5	1.78E5	1.19E4	0.202	96.4	1.37E3	486	1.06	3.48E5	1.79E5	1.24E4	0.208	18.9	88.0	30.3	46.2
30.4	2.59E5	1.32E5	8.87E3	0.201	836	4.21E3	887	0.633	2.6E5	1.36E5	9.76E3	0.215	19.0	85.1	29.5	46.9
34.1	2.06E5	1.06E5	7.16E3	0.202	948	4.4E3	892	0.608	2.07E5	1.11E5	8.06E3	0.219	19.1	82.3	28.8	47.6

* Here and below, $2.44E6 = 2.44 \cdot 10^6$.

Table 2

#	a_S^{acc}	a_V^{acc}	a_S^{md}	a_V^{md}	Δa^{acc}	Δa^{md}	RH, %	Q, $g \cdot m^{-3}$	T, °C
3	0.0233	0.0260	0.0491	0.0445	–0.00270	0.00460	45	6.82	45
4	0.0193	0.0233	0.0609	0.0573	–0.00400	0.00360	70	11.5	18.7
5	0.0242	0.0294	0.0606	0.0531	–0.00517	0.00750	86	14.0	19.1
6	0.0267	0.0292	0.0498	0.0433	–0.00250	0.00650	50	7.80	18.4
7	0.0248	0.0277	0.0348	0.0301	–0.00289	0.00474	65	10.2	18.5
8	0.0257	0.0285	0.0887	0.0925	–0.00279	–0.00380	91	14.7	18.8
9	0.0252	0.0313	0.0435	0.0383	–0.00614	0.00520	51	15.0	31.2

Figure 11 compares the spectra of volume distribution of smoke particles; these spectra were obtained in the series of experiments discussed here. All the data presented in Fig. 11 characterize the disperse structure of smokes by the time of reaching maximum of relative humidity in the measurement cell ($t \approx 20$–22 min).

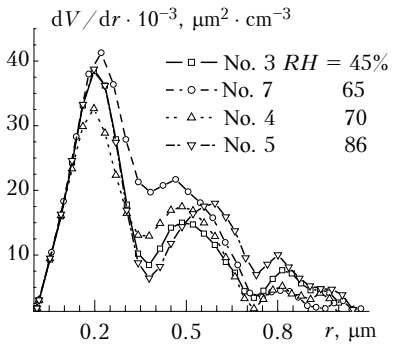

Fig. 11. Deformation of the spectra of volume distribution of smoke particles during variations of relative wetting of air mixture in pyrolysis chamber and spectronephelometer cell in different experiments.

The collected spectra of accumulation fraction agree, primarily because they are obtained for the same type of wood material with fixed mass (380 mg), as well as for nearly similar heating conditions of pyrolysis ($U = 60$ V). At the same time, it is evident, that the variations of pyrolysis conditions, namely relative humidity, cause most marked changes in the spectrum in size range where medium dispersed aerosol fraction forms (Fig. 11). As relative humidity grows, the size spectrum of medium dispersed fraction shifts toward larger values. The stronger the wetting of air mixture, the more effective the particle sink is (see Table 2).

In the main series of experiments, the smoke mixture was carried from pyrolysis chamber to spectronephelometer cell by the method of continuous circulation. The smoke mixture in measurement cell was continuously refreshed from pyrolysis chamber and directed back to it.

In addition to experiments using the method of continuous circulation we also performed a series of measurements in which the smoke mixture was delivered discretely. After a stable signal was achieved in one of the optical channels, a control algorithm of measurements was initiated. Simultaneously, transfer of smoke from pyrolysis chamber to the cell was interrupted. In the course of measurements, the total concentration of smoke aerosols in the spectronephelometer cell gradually decreased. The depletion of the concentration of smoke particles was

accompanied by a decrease of the recorded signals. After reaching minimum permissible (for stable measurements) level of optical signal, a new portion of smoke mixture was pumped into the cell, etc.

The experiments with the use of a few portions of smoke mixture have shown that the rates of kinetic development of disperse composition of smoke in pyrolysis chamber and spectronephelometer cell markedly differ. The particle sink to pyrolysis chamber walls is markedly less effective than the sink to the spectronephelometer cell. This can be easily seen from comparison of relative variations of smoke microstructure parameters at different measurement stages, when a few portions of smoke were used (see Fig. 12*a*).

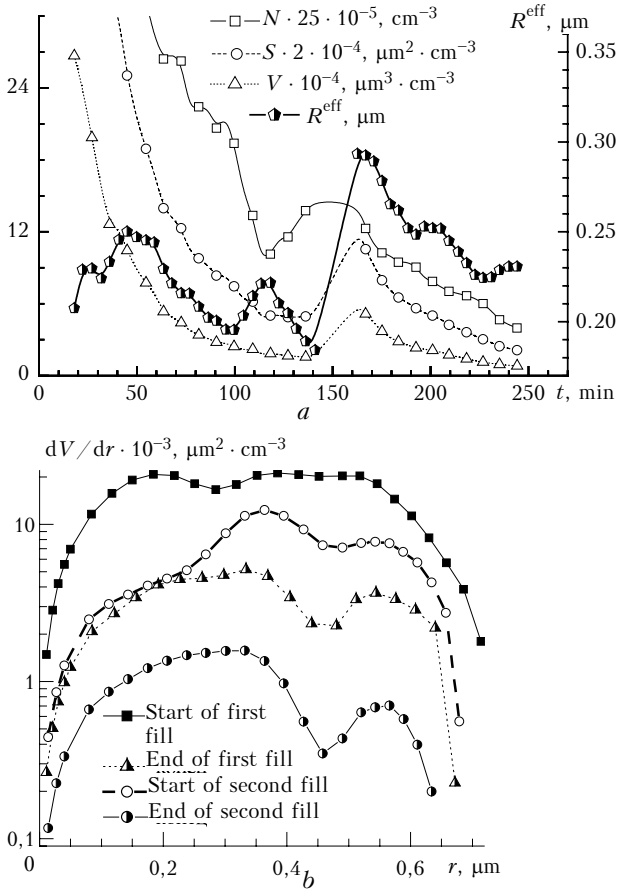

Fig. 12. Variations of microstructure parameters of pyrolysis smokes during double gas fill of spectronephelometer cell: (*a*) integrated characteristics and effective size, (*b*) initial and final size spectra of smoke particles during the first and second fills of the nephelometer cell.

The results presented in Fig. 12*a* also show that, when the number concentration of smoke particles in the first portion was sufficiently high against the background of effective particle sink to the cell walls, distinct features of particle coagulation growth were observed. At the same time, the experiments based on this method show that, during recording of optical characteristics of the first portion, the disperse composition of smoke mixture experiences changes in the shape of size spectrum, and these changes substantially differ in chamber and in the nephelometer cell (Fig. 12, *b*). In process of coagulation development of smoke mixture in pyrolysis chamber, the effective particle size increases by almost a factor of 2–2.5. A distinct feature of the variations of size spectrum in the second portion of smoke mixture in the cell is the steady decrease of effective particle size (see curve *4* after 150 min).

One of the experiments coincided in time with a heavy shower, so that the air mass used for cleaning has been too wet. To reduce the relative humidity, air mixture entering the chamber was subject to additional heating. Approximately half an hour later, examination of signal level from optical channels has revealed a considerable amount of optically detectable aerosol particles, formed in the chamber prior to pyrolysis of the sample. Experiments with preheating of pyrolysis chamber were repeated on a few next days. The recorded signals from optical channels for different scattering angles varied about the level sufficient to identify the angular pattern of scattered radiation (according to its elongation in the forward and backward directions, as well as angular dependence of the polarization degree) as scattering phase function characteristic of aerosol particles.

Figure 14 shows time variations of size spectrum of aerosol particles formed during heating of pyrolysis chamber walls. The time of recording of each curve can be determined from results presented in Fig. 13.

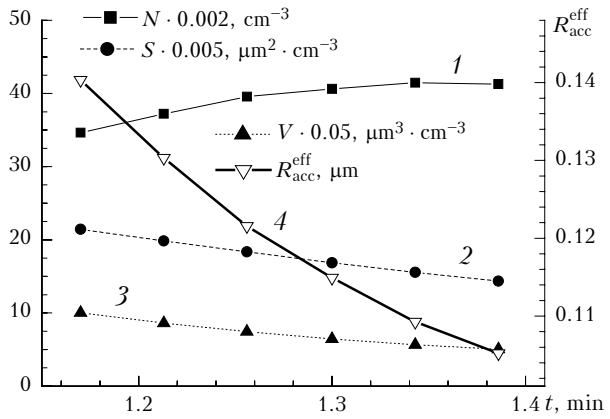

Fig. 13. Variations of integrated parameters of size spectrum, namely N_{acc}, S_{acc}, V_{acc}, and effective size R^{eff}_{acc} of aerosol formed after the pyrolysis chamber was heated to 55°C; the particle size range is 0.05–0.39 μm.

From Fig. 14 we see that the mean size of detected particles is markedly less than the size of smoke aerosol particles. The relative optical contribution of large particles with $r > 0.35$ μm is comparatively small; so the reconstructed spectra have almost no such particles. The real part of refractive index approximately equals the data for wood smokes (1.536), whose thermal sublimation was performed in relatively dry chamber; however, it is significantly less than the refractive index of colophony particles. In time transformation of particle size spectrum we should note that, against the background of effective sink of particles in size range 0.13–0.33 μm, content of particles with $r < 0.1$ μm continues to increase during time period analyzed here.

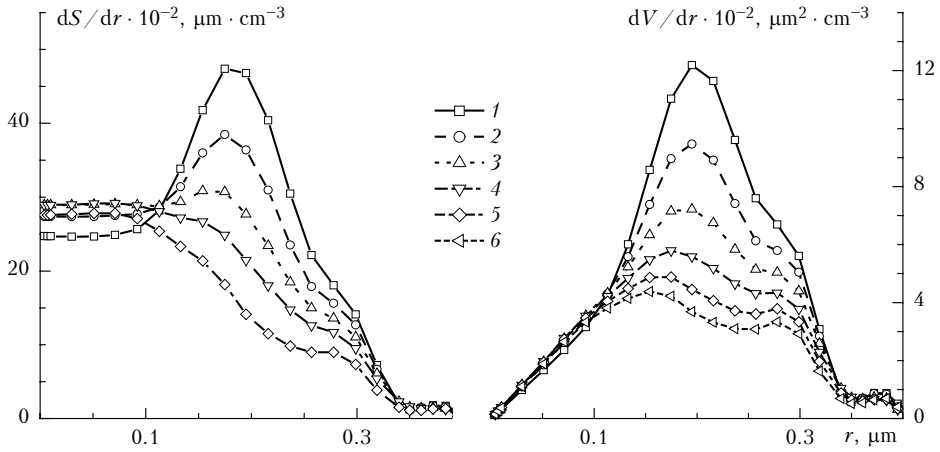

Fig. 14. Time variations of size distribution density function of cross sections and volumes of smoke particles, formed in the experiment only due to heating of pyrolysis chamber; the time of recording of each curve can be determined from data in Fig. 13. Curves *1–6* are drawn through data point of signal recording.

The variations of integrated parameters of size spectrum of aerosol particles, formed only due to heating of chamber, are presented in Fig. 13. Compared with wood pyrolysis smokes, here we see, against the background of increasing number concentration (curve *1*), a steady and faster decrease of effective particle size (curve *4*). Analysis of mutual variations of integrated characteristics (curves *1–3*) shows that, despite vigorous thermophoretic particle sink to the chamber walls (curves *2* and *3* monotonically decrease), a "cold generation" of small particles takes place (curve *1*). As sticking micromonomers migrate from warm smoke stream to air mixture with $T \sim 16$–19°C, they rapidly solidify and form aerosol structures with complex morphology. The number concentration of accumulation-mode particles can increase both due to effective growth of optically inactive ultrafine particles, and as a result of breakdown of weak monomer.

Possibly, the marked decrease of effective particle size may be due to the process of compacting particles with complex morphology. If the chamber is kept at high enough temperature ($T \sim 55$°C) for a long time, the microscopic monomers of tar species present in weak chains preserve the fluidity, facilitating their breaking (by external air flows) into a few smaller chains and mutual sticking of some of them to form more compact structures.

The "cold generation" of small particles has been observed in this experiment only for relatively low concentrations of aerosol particles inside the chamber. For higher number concentrations, the effective particle sink to the chamber walls masks this effect, so that number concentration has a tendency to decrease.

3. Discussion and main conclusions

The obtained experimental data convincingly show that the pyrolysis of coniferous samples leads to a formation of aerosols with a similar microstructure to smokes, formed during thermal sublimation of colophony. The imaginary and real parts of refractive index of wood smokes have properties similar to that of colophony smokes. The observed mismatches are caused by variations of water vapor content in air mixture in the chamber: the higher the absolute moisture content, the less the real part of the refractive index. Despite some specific features of dispersed smoke composition in the size range 0.4–1.2 μm, overall the size spectra, reconstructed from the optical measurements, are qualitatively similar to the colophony smokes in fraction structure. In particular, all spectra generally have a separate fraction with $R_{\text{acc}}^{\text{eff}} \sim 0.1$–0.18 μm. As is well known, the accumulation-mode fraction of atmospheric haze has the same size range. The variability range of disperse composition of smokes in medium dispersed fraction should be separated into two subintervals. Because of aerosol sink to chamber walls, in disperse composition of smokes there occurs quite a rapid depletion of particles with $r > 0.75$ μm. Most of the large-size fraction is removed from disperse composition of smokes approximately in 25–30 min after onset of the pyrolysis process.

At the same time, the experiments have shown that, if the air mixture entering the spectronephelometer cell crosses a region with low temperature, and the relative humidity reaches the dew point, there appear in the ensemble of smoke aerosol particles the particles with optical properties characteristic of water droplets. At the initial stage of the process development, the water droplets are ~ 1.2 μm in size; and subsequently, they are quite rapidly removed (by deposition on chamber walls and tubes delivering air mixture to the cell) from disperse composition of smokes. Instead, in approximately 20–25 min into the pyrolysis process, water droplets in the form of medium dispersed fraction with sizes ~ 0.5–0.85 μm start to appear (see Fig. 10).

The process of generation of optically active aerosol particles, discovered during experiments with heating of wetted air mixture, seems to be a consequence of increase of VABS concentration and intensification of emission of tar from chamber walls. This, in turn, suggests that, even a weak heating of

the surface of coniferous trees, such as by solar radiation (up to temperatures ~ 45–55°C) may lead to more intense emission of coniferous tar in amounts sufficient for generation of aerosol particles of biogenic origin from complex aromatic molecules. Importantly, the results of laboratory studies show that the relative abundance of biogenic component in composition of tropospheric aerosols depends not only on the intensity of VABS emission by wood materials, but also on temperature and wetting condition of air mixture.

Thus, the laboratory experiments, show that, as air mixture (with high content of aerosols and VABS) crosses temperature inhomogeneities many times, it experiences significant phase-kinetic changes of disperse composition, particularly in the size range of medium dispersed fraction.

Acknowledgments

This work is supported by Russian Foundation for Basic Research (Grants No. 00–03–32422–a and 01–05–65197–a).

References

1. R.F. Rakhimov, V.S. Kozlov, E.V. Makienko, and V.P. Shmargunov, Atmos. Oceanic Opt. **15**, No. 4, 292–299 (2002).
2. R.F. Rakhimov, V.S. Kozlov, M.V. Panchenko, A.G. Tumakov, and V.P. Shmargunov, Atmos. Oceanic Opt. **14**, No. 8, 624–628 (2001).
3. I.E. Naats, *Theory of Multifrequency Laser Atmospheric Sensing* (Nauka, Novosibirsk, 1980) 157 pp.
4. A.A. Isakov, Atmos. Oceanic Opt. **12**, No. 1, 20–27 (1999).
5. A.A. Isakov, V.V. Lukshin, and M.A. Sviridenkov, Izv. Akad. Nauk SSSR, Ser. Fiz. Atmos. Okeana **24**, No. 3, 258–261 (1988).
6. S.M. Sakerin, R.F. Rakhimov, E.V. Makienko, and D.M. Kabanov, Atmos. Oceanic Opt. **13**, No. 9, 754–758 (2000).
7. R.F. Rakhimov, S.M. Sakerin, E.V. Makienko, and D.M. Kabanov, Atmos. Oceanic Opt. **13**, No. 9, 759–765 (2000).
8. E.V. Makienko, R.F. Rakhimov, S.M. Sakerin, and D.M. Kabanov, Atmos. Oceanic Opt. **15**, No. 7, 531–540 (2002).